



**HAL**  
open science

# **Influence of number of azo bonds and mass transport limitations towards the elimination capacity of continuous electrochemical process for the removal of textile industrial dyes**

Jaanavee Alagesan, Mecghasri Jaisankar, Sindhu Muthuramalingam,  
Emmanuel Mousset, Padmanaban Velayudhaperumal Chellam

## ► To cite this version:

Jaanavee Alagesan, Mecghasri Jaisankar, Sindhu Muthuramalingam, Emmanuel Mousset, Padmanaban Velayudhaperumal Chellam. Influence of number of azo bonds and mass transport limitations towards the elimination capacity of continuous electrochemical process for the removal of textile industrial dyes. *Chemosphere*, 2021, 262, pp.128381. 10.1016/j.chemosphere.2020.128381 . hal-02993294

**HAL Id: hal-02993294**

**<https://hal.science/hal-02993294>**

Submitted on 5 Dec 2020

**HAL** is a multi-disciplinary open access archive for the deposit and dissemination of scientific research documents, whether they are published or not. The documents may come from teaching and research institutions in France or abroad, or from public or private research centers.

L'archive ouverte pluridisciplinaire **HAL**, est destinée au dépôt et à la diffusion de documents scientifiques de niveau recherche, publiés ou non, émanant des établissements d'enseignement et de recherche français ou étrangers, des laboratoires publics ou privés.

1 **Influence of number of azo bonds and mass transport limitations**  
2 **towards the elimination capacity of continuous electrochemical**  
3 **process for the removal of textile industrial dyes**

4  
5 *Jaanavee Alagesan<sup>1</sup>, MecghaSri Jaisankar<sup>1</sup>, Sindhu Muthuramalingam<sup>1</sup>,*

6 *Emmanuel Mousset<sup>2\*</sup>, Padmanaban Velayudhaperumal Chellam<sup>1\*</sup>*

7 *(All authors have equally contributed)*

8  
9 *1- Centre for Research, Department of Biotechnology,*  
10 *Kamaraj College of Engineering & Technology,*  
11 *Madurai, Tamilnadu, India.*

12 *2- Laboratoire Réactions et Génie des Procédés,*  
13 *UMR CNRS 7274, Université de Lorraine,*  
14 *1 rue Grandville BP 20451, 54001 Nancy cedex, France.\**

15  
16 **Accepted version**

17 **Chemosphere**

18  
19 Author to whom correspondence should be addressed

20 *V.C.Padmanaban*  
21 [vcpadmanaban88@gmail.com](mailto:vcpadmanaban88@gmail.com);

22  
23 *Emmanuel Mousset*  
24 [emmanuel.mousset@univ-lorraine.fr](mailto:emmanuel.mousset@univ-lorraine.fr);

27

28 **ABSTRACT**

29 This study focusses on the electrochemical decomposition of synthetic azo dyes (RO16,  
30 RR120 and DR80) using stainless steel electrodes, which is efficient, cost effective and  
31 industrially driven process. The experiments were carried out in a continuous electrochemical  
32 reactor and the effects of influencing parameters (initial concentration of dye, electrolyte  
33 concentration, pH) governing the process efficiency was studied. The interaction between the  
34 influencing parameters was investigated using Response Surface Methodology (RSM) and the  
35 regression value obtained for the generated model was above 0.9 for all the three dyes. The  
36 elimination capacity of electrochemical reactor was studied for the continuous removal of azo  
37 dyes with different ranges of concentration (100 - 400 mg L<sup>-1</sup>) and flow rate (0.1 - 0.5 L h<sup>-1</sup>).  
38 The maximum elimination capacity was obtained at a flow rate of 0.5 L h<sup>-1</sup> for 300 mg L<sup>-1</sup> of  
39 initial concentration of dye for RO16 and RR120 whereas it was 0.5 L h<sup>-1</sup> for 400 mg L<sup>-1</sup> of  
40 DR80. Further, a general dimensionless current density relation has been established for stirred  
41 tank reactor and allowed characterizing the relationship between kinetics and mass transport  
42 contributing to the overall reaction rate. The results quantitatively confirmed that the rate of  
43 electrochemical decolorization increased with the increasing initial dye concentration and flow  
44 rate due to the mass transport limitation. As newly established, the decolorization is also  
45 directly linked to the number of azo bonds.

46

47 **Keywords:** *Azo dyes; Electrochemical process; Response Surface Methodology; Continuous*  
48 *mode; Elimination capacity; Dimensionless current density*

49

50

51

## 52 1. INTRODUCTION

53 Rapid industrialization, continuous growth of population and over exploitation of natural  
54 resources has created an imbalance in the ecosystem. It has also intensified the environmental  
55 issues associated with water, air and land. Enormous increase in the growth and development  
56 of industries created a global demand for water due to its excessive consumption as it cannot be  
57 substituted for its wide range of industrial applications. But the prevailing water crisis has  
58 created an increasing awareness on the limited access to freshwater resources. The United  
59 Nations World Water Development report released in 2018, forecasts that by the year 2050  
60 nearly 3.6 to 4.6 billion people will be facing severe water stress.

61 On the other hand, due to the negligence in the implementation of stringent policies  
62 towards industrial water treatment as well as lack of efficient technologies in large scale has  
63 created an another dimension of water stress in terms of quality. Large amount of water and  
64 chemicals are consumed by the textile hubs for the wet processing of materials and  
65 simultaneously significant volume of contaminated effluent is discharged (Hasanbeigi and  
66 Price, 2015). Consumption of such contaminated resources will have a direct impact on the  
67 health status of the human. Among such micropollutants, azo dyes creates a major havoc to the  
68 environment and the public health because of their toxic nature due to the presence of aromatic  
69 amine groups (Holkar et al., 2016). Schneider et al., reported on the mutagenic nature of textile  
70 dyes by studying the genotoxic activity of azo dyes (Schneider et al., 2004). Additionally,  
71 allergic contact dermatitis and respiratory diseases are known to be caused by textile dyes  
72 (Gürses et al., 2016). However, azo dyes are predominantly used by majority of the Indian  
73 textile industries as it is economic and also acts as an effective chromophore. The available  
74 literature demonstrates an extensive number of treatment methodologies involving physical  
75 methods like adsorption (Brahmi et al., 2019; Shahnaz et al., 2020a, 2020b; Sharma et al.,  
76 2020), chemical (Jegan Durai et al., 2020) and biological processes (Padmanaban et al., 2016)

77 as well as some of the new emerging techniques like advanced oxidation process and  
78 photoelectrocatalysis (Aquino et al., 2013). Though there are plethora of research publications  
79 on developing process for the decolorization of textile dyes, still in industries those  
80 technologies are not in practice. Most of the developed process in the laboratory conditions  
81 fails during scale up or during experimenting with real industrial effluent. The possible reasons  
82 could be: (a) process development using pH indicators and stains; (b) the industrial effluent is a  
83 complex mixture of different classes of dyes like monoazo, diazo, polyazo, Reactive and  
84 Direct; (c) the industrial effluent pH is alkaline in nature; (d) high salt concentration in the  
85 industrial effluent; (e) large volumes to handle at short time, i.e. high treatment capacity  
86 requirement. To face these multiple constraints, developing a cost-effective technology remain  
87 a challenge. A streamlined approach need to be followed during the process development for  
88 the decolorization or degradation of dyes by using chemical engineering tools and  
89 methodology.

90 Over the past decades, electrochemical processes have gained an increasing interest among  
91 the environment researchers in treating various micro and macro pollutants from various  
92 industries and especially dyes (Brillas and Martínez-Huitle, 2015). In direct electrolysis, at the  
93 anodic surface, direct exchange of electrons takes place with the pollutants, thereby it  
94 destabilises or degrade the pollutants whereas in indirect electrolysis, the exchange of electrons  
95 with the pollutants is mediated by active species. The chain of redox catalysis takes place from  
96 anodic surface to pollutants through series of electroactive species generated reversibly or  
97 irreversibly (Panizza and Cerisola, 2009). Non-active anodes can even produce physisorbed  
98 hydroxyl radicals ( $\cdot\text{OH}$ ) that are available for indirect oxidation of the majority of organic  
99 compounds that can enhance the degradation and mineralization efficiency (Mousset et al.,  
100 2018). Upon the superiority of this mechanism, numerous articles proposed their  
101 implementation for dyes elimination (Brillas and Martínez-Huitle, 2015). However, such

102 advanced electro-oxidation processes involve expensive materials such as boron-doped  
103 diamonds (BDD) materials that proved to be currently the best option for long-term and real  
104 applications (Nidheesh et al., 2019). Contrastingly, when using active anode, i.e. without  
105 available  $\cdot\text{OH}$  for indirect oxidation, the electrochemical degradation of dyes wastewater could  
106 still occur, mainly by electron transfer reaction coupled with a dissociation chemisorption step  
107 (Mohan et al., 2007). The efficiency of direct anodic oxidation of dyes benefits from the  
108 presence of several functional groups (e.g. azo bonds) on their molecules that make them  
109 electroactive for direct electron transfer (Michaelis, 1935). Moreover, the advantage of active  
110 anodes (e.g. graphite, stainless steel) is their low cost compared to non-active materials, while  
111 their efficiency towards dyes removal could remain still competitive in terms of cost-efficiency  
112 (Mohan et al., 2007). This type of oxidation has been further tested as a viable alternative for  
113 the degradation of textile dyes owing to their cost-effectiveness, eco-friendly nature and ability  
114 to produce less sludge (Bassyouni et al., 2017). Moreover, electrocoagulation process has also  
115 demonstrated to be effective for dye wastewater treatment by using cheap aluminium or iron  
116 based- sacrificial anode for coagulant generation (Arslan-Alaton et al., 2008). A synergy by  
117 using a non-active anode such as stainless steel that can act both as sacrificial anode and as a  
118 role of direct electro-oxidation could be therefore interesting (Arslan-Alaton et al., 2008). The  
119 presence of chloride at sufficient high concentration ( $> 0.6 \text{ g L}^{-1}$ ) has shown to favour both the  
120 mediated oxidation with active chlorine ( $\text{Cl}_2$ ,  $\text{ClOH}$ ) and the electrocoagulation mechanism  
121 with iron-based anode (Hakizimana et al., 2017). Since dye effluents contain high content of  
122 chloride, this could be interesting to combine electro-oxidation with electrocoagulation for  
123 such application (Hakizimana et al., 2017).

124 In order to proceed with this approach, better understanding on the electrochemical process,  
125 the influence of molecular structure of dyes as well as the competition study between charge  
126 transfer and mass transport is required for such heterogeneous process. The main objective of

127 this study is therefore to provide answers to these issues for the first time, by developing a  
128 continuous stirred electrochemical reactor for the decolorization of textile dyes having different  
129 number of azo bonds. An optimization of the technology is first proposed, by using One  
130 Variable At a Time approach (OVAT) and Response Surface Methodology (RSM) in batch  
131 mode. Then the effectiveness of the process in terms of elimination capacity, current efficiency  
132 and energy consumption has been assessed under continuous mode. A general expression of  
133 dimensionless current density is suggested for stirred tank cell design, as a way of better  
134 quantitatively describe the competitiveness between charge transfer and mass transport  
135 phenomena.

136

## 137 **2. MATERIALS AND METHODS**

### 138 **2.1. Chemicals used**

139 In this study, industrially used azo bond containing dyes of different classes were used.  
140 Reactive Orange 16 (RO16), Reactive Red 120 (RR120) and Direct Red 80 (DR80) were taken  
141 as the model dyes and were procured from Sigma-Aldrich, India. The physico-chemical  
142 properties of the dyes are given in Table SM-1. Other chemicals such as sodium chloride  
143 (NaCl), hydrochloric acid (HCl) and sodium hydroxide (NaOH) of laboratory grade were  
144 purchased from HiMedia Laboratories, India. Simulated dye solution was prepared by  
145 dissolving the industrially used azo dyes (RO16, RR120 and DR80) in aqueous medium and  
146 was diluted to the specified concentration as released in the industrial effluent. Sodium chloride  
147 is used as the supporting electrolyte in the process, since  $\text{Cl}^-$  is a predominant inorganic species  
148 at high concentration in most of dyes effluents (Hakizimana et al., 2017). The pH of the  
149 solution was adjusted using 1 N NaOH (basic) and 1 N HCl (acidic).

150

151

## 152 2.2. Electrochemical reactor and dye decolorization analysis

153 A cylindrical lab scale reactor made up of borosilicate glass with a net volume of 1500  
154 cm<sup>3</sup> was used for the electrochemical decolorization of synthetic wastewater. Stainless steel  
155 electrodes (both anode and cathode) (Kristeel brand) with an immersed surface area of 17 cm<sup>2</sup>  
156 were used. The inter-electrode distance between the anode and cathode was fixed as 4 cm for  
157 all the experimental runs. For all the experiments the voltage was maintained within the ranges  
158 of 3.8 - 4.0 V (previous unpublished data) using a variable DC power supply (Scientech  
159 Technologies), corresponding to an average applied current density of 47 mA cm<sup>-2</sup>. These  
160 values fall in the range of optimal current density found in a previous study using stainless steel  
161 sacrificial anode for dye wastewater (Arslan-Alaton et al., 2008). A magnetic stirrer (Remi)  
162 was used for the stirring of solutions (100 rpm). The experiments were conducted at room  
163 temperature. Block diagram of the electrochemical reactor is shown in the graphical abstract.  
164 Sludge were also generated during the electrocoagulation mechanism at the stainless steel  
165 anode, according to Eq. (1) and Eq. (2) (Arslan-Alaton et al., 2008):



168 The sludge was then separated using centrifugation at 8000 rpm for 5 min. The decolorization  
169 of dyes was monitored by change in absorbance and measured  $\lambda_{\text{max}}$  as specified in the Table  
170 SM-1 using a UV-Visible spectrophotometer (Eppendorf, Germany). The percentage of  
171 decolorization and concentration of dye decolorized were calculated based on Eq. (3):

$$172 \quad \% \text{ removal in terms of decolorization} = \left( \frac{A_i - A_t}{A_i} \right) \times 100 \quad (3)$$

173 where  $A_i$  and  $A_t$  are absorbance at initial time and absorbance at time  $t$ , respectively.

174

175

176

177 **2.3. Batch process optimization – OVAT**

178 A batch mode was chosen as a preliminary step to determine the effects of pH,  
179 electrolyte concentration and initial concentration of dye on the electrochemical decolorization  
180 of synthetic wastewater. This investigation was carried out in order to determine the optimum  
181 operating conditions for achieving maximum percentage of dye decolorization. For better  
182 understanding of the influencing factors, individual set of experiments were performed for all  
183 the three dyes (RO16, RR120 & DR80) within the specified range of reaction conditions (pH:  
184 3.0 - 11.0, electrolyte concentration: from 0.1 to 0.5 M and initial concentration of dye: from  
185 100 to 500 mg L<sup>-1</sup>). Working volume of 500 mL was fixed for all experiments. The treated  
186 samples collected at periodic time intervals were subjected to centrifugation (5000 rpm, 5 min)  
187 for separating the sludge particles generated during the electrochemical process.

188

189 **2.4. Batch process optimization – RSM**

190 RSM is one of the structured statistical methods for designing experiments, generating  
191 models, understanding variable effects on the response and also for improving the response  
192 using optimal conditions (Amani-ghadim et al., 2013). In this study, modified face centred  
193 central composite design (CCF) with alpha value 1.0 was used to analyze the interaction  
194 between the influencing parameters and also on the selection of optimum variables for  
195 maximizing the decolorization of synthetic azo dyes. Initial concentration of dye, pH and  
196 reaction time for the electrochemical process were the selected factors to be studied using  
197 RSM. In case of direct dyes, pH was excluded as it had no significant effects on decolorization.  
198 The experimental design for the decolorization of azo dyes is shown in Table 1.

199

200

201

**Table 1** Experimental design for decolorization of azo dyes by RSM-CCF

<b>a) Reactive dyes (RO16 and RR120)</b>					
<b>Factor</b>	<b>Units</b>	<b>Low Actual</b>	<b>High Actual</b>	<b>Mean</b>	<b>Std. Dev</b>
<b>A</b> = Initial concentration of dye	mg L <sup>-1</sup>	100	1000	550	318.29
<b>B</b> = pH	-	3.0	11.0	7.0	2.828
<b>C</b> = Time	min	5	15	10	3.536
<b>Response</b>	<b>Units</b>	<b>Model</b>	<b>Transformation</b>	<b>Mean</b>	<b>Ratio</b>
<b>Y<sub>1</sub></b> = Concentration of RO16 decolorized	mg L <sup>-1</sup>	Quadratic	Base 10 log	204.52	57.496
<b>Y<sub>2</sub></b> = Concentration of RR120 decolorized	mg L <sup>-1</sup>	Quadratic	Inverse Sq Rt	265.27	12.89
<b>b) Direct dye (DR80)</b>					
<b>Factor</b>	<b>Units</b>	<b>Low Actual</b>	<b>High Actual</b>	<b>Mean</b>	<b>Std. Dev</b>
<b>A</b> = Initial concentration of dye	mg L <sup>-1</sup>	100	1000	550	318.29
<b>B</b> = Time	min	5	15	10	3.536
<b>Response</b>	<b>Units</b>	<b>Model</b>	<b>Transformation</b>	<b>Mean</b>	<b>Ratio</b>
<b>Y<sub>3</sub></b> = Concentration of DR80 decolorized	mg L <sup>-1</sup>	Quadratic	Power	492.79	10.88

202

203

204

## 205 **2.5. Decolorization of azo dyes – Continuous process**

206 The decolorization of the azo dyes was monitored during continuous electrochemical  
207 treatment. The simulated dye solution was pumped into the continuous reactor via peristaltic  
208 pump with a predetermined flow rate (ranging from 0.1 to 0.5 L h<sup>-1</sup>). For all the experimental  
209 runs, hold-up volume of the reactor was maintained as 700 mL by providing similar flow rates  
210 at both the inlet and outlet. This experiment was performed with various dye concentrations  
211 (100, 200, 300 and 400 mg L<sup>-1</sup>) at pH 11.0 for all the three dyes. The electrolyte (salt)  
212 concentration was maintained using 0.5 M NaCl. The reactor efficiency was calculated by the  
213 elimination capacity for different inlet loading rates using Eq. (4) and Eq. (5).

$$214 \quad \text{Inlet loading rate (mg (Lh)}^{-1}\text{)} = \frac{C_{in}Q}{V} \quad (4)$$

$$215 \quad \text{Elimination capacity (mg (Lh)}^{-1}\text{)} = \frac{(C_{in}-C_{out})Q}{V} \quad (5)$$

216 where C<sub>in</sub> and C<sub>out</sub> are inlet and outlet concentration of dye respectively, Q is the  
217 volumetric flow rate (L h<sup>-1</sup>) and V is the holdup volume of the reactor (L).

218

## 219 **3. RESULTS AND DISCUSSION**

### 220 **3.1. Characterization of dye – Changes in absorption spectra**

221 The characterization and the suitability of the kinetics of dye decolorization assessment by the  
222 spectrophotometric method is carried out as a preliminary step. 100 mg L<sup>-1</sup> of simulated  
223 solution was prepared individually for all the three dyes (Operating conditions: pH 11.0, 0.5 M  
224 NaCl, 4 V) and subjected to electrochemical process for 10 min. The result of changes in  
225 absorption spectra of samples before decolorization (0<sup>th</sup> min) and after decolorization is shown  
226 in the Fig. SM-1. The UV-Visible spectrophotometric analysis of non-decolorized RO16 dye  
227 shows two prominent peaks at 490 nm and 390 nm, RR120 shows at 510 nm and 290 nm and  
228 DR80 shows at 540 nm and 290 nm respectively. The peak in the visible region corresponds to  
229 the conjugated structure of azo bond (chromophores) and peak in the UV region is attributed to

230 the aromatic structure (Padmanaban et al., 2018). The dye solutions subjected to  
231 electrochemical process lost its colour and it is confirmed from the disappearance of prominent  
232 peaks without apparition of interfering peaks that could come from the matrix and  
233 intermediates generated with electrolysis time. It further confirms the reliability to use this  
234 method for the following batch and continuous mode studies, by considering that the  
235 absorbance measured at wavelength giving maximal absorbance of the dye was link only to the  
236 concentration of the studied dye and not to any other species that could absorb also at this  
237 wavelength.

238

### 239 **3.2. Batch process optimization – OVAT**

240 Most textile industries produce effluent that need to be neutralized from highly alkaline pH  
241 prior to discharge or reuse. With respect to effluent treatment plants, the pH of the influent  
242 coming to the plants may be of diverse range of pH and it has to be brought near to the pH of  
243 the process employed in the treatment plant. The effect of pH (3.0 - 11.0) on the process of  
244 decolorization was studied through five different batch experiments at 100 mg L<sup>-1</sup> of initial  
245 concentration of dyes (RO16, RR120 & DR80) with 0.5 M of electrolyte concentration at 4 V.  
246 At 6<sup>th</sup> min, the process of decolorization comes to an equilibrium. Table 2 depicts the  
247 percentage of dye decolorization at 6<sup>th</sup> min for different pH. For the reactive and direct dyes,  
248 percentage of decolorization increased while moving from acidic condition to alkaline  
249 condition. Close examination of the results indicates that nearly 100% of decolorization was  
250 achieved at pH 11.0. At pH > 7.5, the rate of Fe<sup>2+</sup> oxidation into Fe(OH)<sub>2</sub>(s) (Eq. (6)) is  
251 increased, which subsequently increase the production of Fe(OH)<sub>3</sub>(s) (Eq. (7)) and can  
252 therefore increase the electrocoagulation efficiency (Hakizimana et al., 2017).

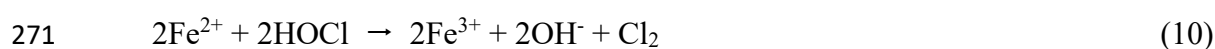


255 Knowing that the pH of majority of textile wastewaters (cotton fibre) lies within the range 8.0-  
256 12.0 (Correia et al., 1994), pH adjustment won't be required to operate at optimal pH. Hence,  
257 pH 11.0 is considered to be the optimum pH for the decolorization of azo dyes by  
258 electrochemical process with the employment of stainless steel electrodes.

259 The effect of electrolyte was studied at various concentrations ranging from 0.1 to 0.5 M  
260 NaCl. From Table 2, it is shown that the percentage of decolorization for the solution with an  
261 initial dye concentration of 100 mg L<sup>-1</sup> and pH 11.0 increases with the increasing electrolyte  
262 concentration. Eq. (8) and Eq. (9) shows that the active chlorine species (Cl<sub>2</sub>, ClOH) (Mousset  
263 et al., 2020)) generated from Cl<sup>-</sup> oxidation could have contributed in the indirect  
264 electrochemical process of azo dyes:



267 Similar kinds of results have been also reported with active anode that was not made of  
268 mixed metal oxide but with a carbon-based material (Mousset et al., 2020). In addition, the  
269 formation of active chlorine has shown to increase the formation of Fe<sup>3+</sup> (Eq. (10)), that then  
270 enhance the electrocoagulation process (Hakizimana et al., 2017):



272 For reactive dyes, 0.5 M NaCl was the optimum electrolyte concentration for achieving  
273 100% of dye decolorization, while the maximum of decolorization was already reached at  
274 0.3M with DR80. Therefore, the supporting electrolyte concentration was fixed at 0.5 M for the  
275 subsequent experiments as the real time textile industrial effluent has a mixture of reactive and  
276 direct dyes. This is further representative of the range of concentrations given in real dye  
277 wastewater (Arslan-Alaton et al., 2008).

278

279

**Table 2** Decolorization of azo dyes – One Variable At a Time approach: Effect of pH, Effect of Electrolyte Concentration (NaCl), Effect of Initial Concentration of dye

<b>pH</b>	<b>% of dye decolorized</b>		
	<b>RO16</b>	<b>RR120</b>	<b>DR80</b>
3.0	53	79	84
5.0	57	89	86
7.0	61	85	90
9.0	87	93	98
11.0	100	97	100

*Initial conc. of dye = 100 mg L<sup>-1</sup>; Electrolyte concentration = 0.5 M;  
Voltage = 4 V; Run time = 6 min*

<b>Electrolyte Concentration (M)</b>	<b>% of dye decolorized</b>		
	<b>RO16</b>	<b>RR120</b>	<b>DR80</b>
0.1	18	9	39
0.2	21	33	72
0.3	23	63	100
0.4	47	83	100
0.5	90	100	100

*Initial concentration of dye = 100 mg L<sup>-1</sup>; pH = 11.0;  
Voltage = 4 V; Run time = 6 min*

<b>Initial Concentration of dye (mg L<sup>-1</sup>)</b>	<b>Concentration of dye decolorized (mg L<sup>-1</sup>)</b>		
	<b>RO16</b>	<b>RR120</b>	<b>DR80</b>
100	100	99	100
200	90	115	199
300	117	119	300
400	107	122	391
500	164	240	488

*pH = 11.0; Electrolyte concentration = 0.5 M;  
Voltage = 4 V; Run time = 6 min*

280

281 The effect of initial concentration of dye on the decolorization of azo dyes by  
282 electrochemical process was studied by varying the concentrations from 100 to 500 mg L<sup>-1</sup>.  
283 The results from Table 2 explains the decolorization potential of the process with respect to  
284 different dyes. The concentration of dye decolorized increased with increase in the  
285 concentration of azo dyes. At high initial concentration of dye (500 mg L<sup>-1</sup>), 33% (164 mg L<sup>-1</sup>)

286 of RO16 and 48% (240 mg L<sup>-1</sup>) of RR120 were decolorized, whereas 97% of DR80 (488 mg L<sup>-1</sup>) was removed. From this study, it is interesting to note that as the complexity of dye increases  
287 with respect to number of azo bonds, the kinetics of decolorization is raising, as further  
288 discussed in section 3.4.  
289

290 In addition, the amount of generated sludge was around 5.1 g h<sup>-1</sup> in optimal condition,  
291 which is not negligible and highlighted the contribution of electrocoagulation mechanism in the  
292 removal efficiency. Still, the amount of sludge produced was 3 times less than with aluminium  
293 sacrificial anode in another study to reach complete colour removal (Arslan-Alaton et al.,  
294 2008).

295

### 296 **3.3 Batch process optimization – RSM**

#### 297 **3.3.1 Experimental design and statistical analysis**

298 The effect of interaction between the influencing factors on the decolorization of the  
299 azo dyes (RO16, RR120, DR80) by electrochemical process and the design parameters based  
300 on the RSM-CCF are shown in Eqs. (11) - (13). Based on RSM designs for all the three dyes,  
301 the data were fitted into the second order polynomial equation and the empirical relationship  
302 between the dependent and independent parameters involved in the decolorization of dyes were  
303 established.

$$304 \text{ Concentration of RO16 dye decolorized} = +228.02 + 74.27A + 56.58B + 78.00C + 27.26AB + \\ 305 52.51AC + 8.26BC - 38.24A^2 - 25.80B^2 - 47.77C^2 \quad (11)$$

$$306 \text{ Concentration of RR120 dye decolorized} = +323.44 + 122.31A + 53.32B + 97.87C + 46.98AB \\ 307 + 77.02AC + 26.21BC - 108.59A^2 + 16.03B^2 - 23.76C^2 \quad (12)$$

$$308 \text{ Concentration of DR80 dye decolorized} = +549.41 + 360.54A + 99.24B + 123.16AB - \\ 309 47.69A^2 - 74.99B^2 \quad (13)$$

310 Box-Cox plots and diagnostic plots for RO16, RR120 and DR80 are given in the  
 311 supplementary data Fig. SM-2, SM-3 and SM-4 respectively. The Box-Cox transformation has  
 312 been employed to improve the normality of residuals and the plots suggested a transformation  
 313 in all the models: Base 10 logarithmic transformation for RO16, Inverse square root  
 314 transformation for RR120, Power transformation for the DR80. The transformed and reduced  
 315 model equations are given in Eqs. (14) - (16).

$$316 \text{Log}10(\text{Concentration of dye decolorized}) = +2.32 + 0.30A + 0.29B + 0.36C - 0.18BC - 0.29B^2 \\ 317 - 0.23C^2 \quad (14)$$

$$318 1.0/\text{Sqrt}(\text{Concentration of dye decolorized}) = +0.055 - 0.024A - 6.946E-003B - 0.014C + \\ 319 3.863E-003BC + 0.024A^2 + 8.460E-003C^2 \quad (15)$$

$$320 (\text{Concentration of dye decolorized})^{0.5} = +23.40 + 9.32 A + 1.92 B + 2.29AB - 3.52 A^2 - 1.52 \\ 321 B^2 \quad (16)$$

322 Analysis of variance (ANOVA) for the RSM models of all the three dyes are  
 323 consolidated in the Table 3 and supplementary data are shown in the Table SM-2, Table SM-3  
 324 and Table SM-4. The significance of each coefficient can be determined by the F-value and p-  
 325 values. The effect on the response increases with larger magnitude of F-values and smaller P-  
 326 values. The P-Value of models generated for all the three dyes is less than 0.0001 and this  
 327 indicates the significance of the parameters in the model. From the results, it was observed that  
 328 for the decolorization of RO16, three linear terms (A, B, C), two quadratic terms ( $B^2$ ,  $C^2$ ) and  
 329 an interactive term (BC) are determining, whereas for the decolorization of RR120, three linear  
 330 terms (A, B, C), two quadratic terms ( $A^2$ ,  $C^2$ ) and an interactive term (BC) are significant. For  
 331 all the three dyes, diagnostic plots such as predicted versus experimental helps to judge the  
 332 adequacy and significance of the model. Normality of the residuals is determined using the  
 333 normal probability plot. In this plot, the distribution of the residuals lies close to the trend lines  
 334 and this shows minimum disperse effect. Though the lack of fit in the model is significant for

335 RO16 and DR80, all the centre point experiments are performed independently for all the three  
 336 dyes to study the fitness of the model with respect to other error analysis parameters which  
 337 suggest the model is fit in respective transformations (Muniyasamy et al., 2020).

338

**Table 3** CCF Model parameters for the decolorization of azo dyes from the  
 Analysis of Variance

<b>Parameters</b>	<b>RO16</b>	<b>RR120</b>	<b>DR80</b>
Model (P-value)	<0.0001	<0.0001	<0.0001
Significant Parameters & Interactions	A, B, C, BC, B <sup>2</sup> , C <sup>2</sup>	A, B, C, BC, A <sup>2</sup> , C <sup>2</sup>	A, B, AB, A <sup>2</sup> , B <sup>2</sup>
R <sup>2</sup>	0.9277	0.9856	0.9879
Adjusted R <sup>2</sup>	0.8943	0.9790	0.9792
Adequate Precision	20.32	40.365	32.645
Coefficient of variation (%)	7.74	5.34	4.97

339

### 340 3.3.2 Analysis of response surface – Operational parameters

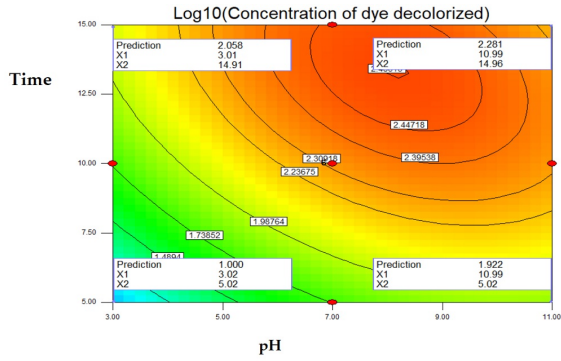
341 The interactive effects between operational parameters are explained by two dimensional  
 342 (contour) and three dimensional plots as shown in Fig. 1.

#### 343 *Interactive effects of pH and time*

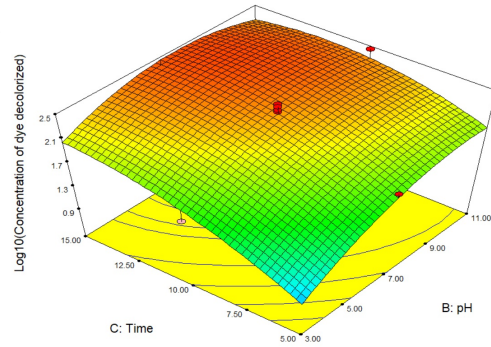
344 The interactive effects between pH and time are significant in the decolorization of reactive  
 345 dyes (RO16, RR120). From the contour plot of RO16 (Figs. 1a and 1b), it can be interpreted  
 346 that maximum concentration of dye decolorization was obtained at alkaline pH and at a  
 347 reaction time for about 15 min. In the case of RR120 (Figs. 1c and 1d), at pH 11.0 the  
 348 concentration of dye decolorization increased from 223 to 494 mg L<sup>-1</sup> with respect to the

349 increase in time from 5 to 13 min. Thus, for both reactive dyes increase in pH and time has  
 350 maximized the concentration of dye decolorization.

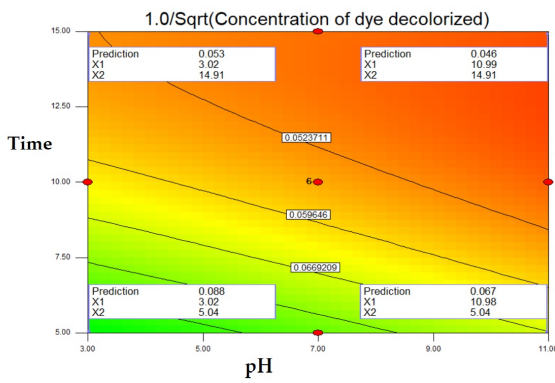
a



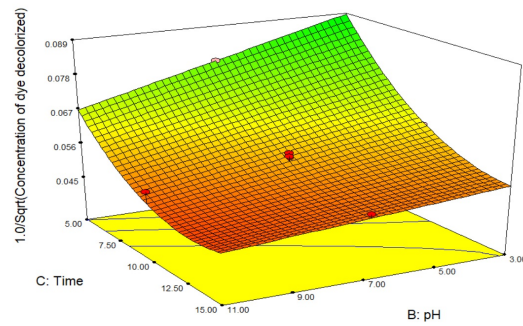
b



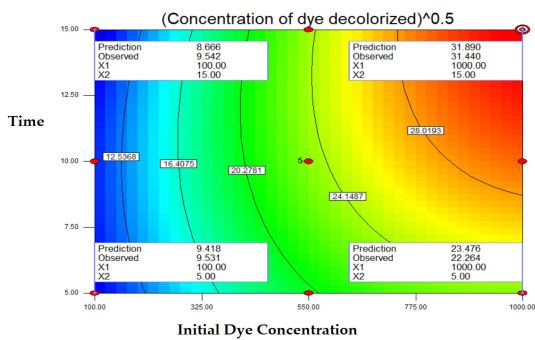
c



d



e



f

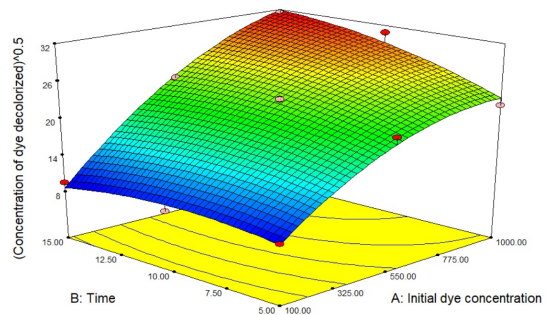


**Fig. 1** CCF based Contour 2D and 3D Response surface plots: RO16 (a&b), RR120 (c&d) and DR80 (e&f)

351

352

### 353 *Interactive effects of initial concentration of dye and time*

354 The interactive effects between initial concentration of dye and time are significant in the  
355 decolorization of DR80 (Figs. 1e and 1f). Maximum concentration of dye decolorization was  
356 obtained with an increase in both the initial concentration of dye and time. The concentration  
357 of dye decolorized increased from 703 to 989 mg L<sup>-1</sup> during 10 to 15 min with an increase in  
358 the initial concentration of dye from 550 to 1000 mg L<sup>-1</sup>.

359

### 360 **3.4 Electrochemical treatment of azo dyes under continuous mode**

361 The elimination capacity of continuous electrochemical treatment was studied for all  
362 the three dyes with different concentrations (100 - 400 mg L<sup>-1</sup>), at varied flow rates (0.1 - 0.5 L  
363 h<sup>-1</sup>). The removal efficiency and elimination capacity of RO16, RR120 & DR80 respectively at  
364 9<sup>th</sup> min was shown in the Table SM-5. The reactor efficiency was calculated using the inlet  
365 loading rate. The results are compared based on the reaction time. In the case of 100, 200 &  
366 300 mg L<sup>-1</sup> of RO16 dye concentration, the elimination capacity increased with the increase in  
367 the inlet loading rate. For 300 mg L<sup>-1</sup> of RO16 with an inlet loading rate of 214 mg (L h)<sup>-1</sup>, the  
368 elimination capacity obtained was 113 mg (L h)<sup>-1</sup> (~ 52% of inlet loading rate is eliminated)  
369 with residence time of 0.531 min. This was observed to be the maximum elimination capacity  
370 for RO16. Similar pattern was observed in RR120. For 300 mg L<sup>-1</sup> of RR120 with an inlet  
371 loading rate of 214 mg (Lh)<sup>-1</sup>, the elimination capacity obtained was 159 mg L<sup>-1</sup> h<sup>-1</sup> (~ 74% of  
372 inlet loading rate is eliminated) with residence time of 0.377 min. Elimination capacity  
373 decreased in the different flow rates of both the reactive dyes (RO16 and RR120) at 400 mg L<sup>-1</sup>  
374 <sup>1</sup>. Interestingly, the maximum elimination capacity of DR80 was observed at 0.5 L h<sup>-1</sup> of 400  
375 mg L<sup>-1</sup> concentration. 99% of inlet loading rate (280 mg (Lh)<sup>-1</sup>) was removed with residence  
376 time of 0.214 min.

377 To further understand the difference between the dyes removal efficiency, their  
378 percentages removal efficiencies have been illustrated in Fig. 2 for different inlet  
379 concentrations (100 - 400 mg L<sup>-1</sup>) and flow rates (0.1 - 0.5 L h<sup>-1</sup>). In all the conditions, the  
380 removal yield of DR80 was higher than RR120, which was higher than RO16. For instance, the  
381 removal efficiency equalled 23%, 48% and 99% at 400 mg L<sup>-1</sup> and 0.5 L h<sup>-1</sup>. Moreover, the  
382 average residence time for 1 mg L<sup>-1</sup> of RO16, RR120 and DR80 was found to be 0.531, 0.377  
383 and 0.214 min respectively (Table SM-6), which corroborated the behaviour. This trend was in  
384 agreement with the results obtained in batch mode, highlighting the influence of number of azo  
385 groups on dye molecule considering that RO16, RR120 and DR80 have 1, 2 and 4 azo bonds,  
386 respectively (Table 2). Thus, the higher the number of azo groups, the better the removal  
387 efficiency. Interestingly, a linear relation was newly obtained between the number of azo bonds  
388 and the removal efficiency as well as with the elimination capacity, giving slope values of 24.4  
389 ( $R^2 = 0.9988$ ) and 70.0 ( $R^2 = 0.9988$ ), respectively (Fig. 3a). Moreover, the increase of inlet  
390 concentration makes increase the removal efficiencies for RO16 and RR120, while the removal  
391 efficiencies of DR80 were around  $97.5 \pm 2.5\%$  for all the inlet concentrations. This means that  
392 the kinetics were depending on the inlet concentrations. Another interesting feature is that the  
393 removal efficiency was increasing with the flow rate, i.e when the retention time was  
394 decreasing, for all the dyes whatever their inlet concentrations.

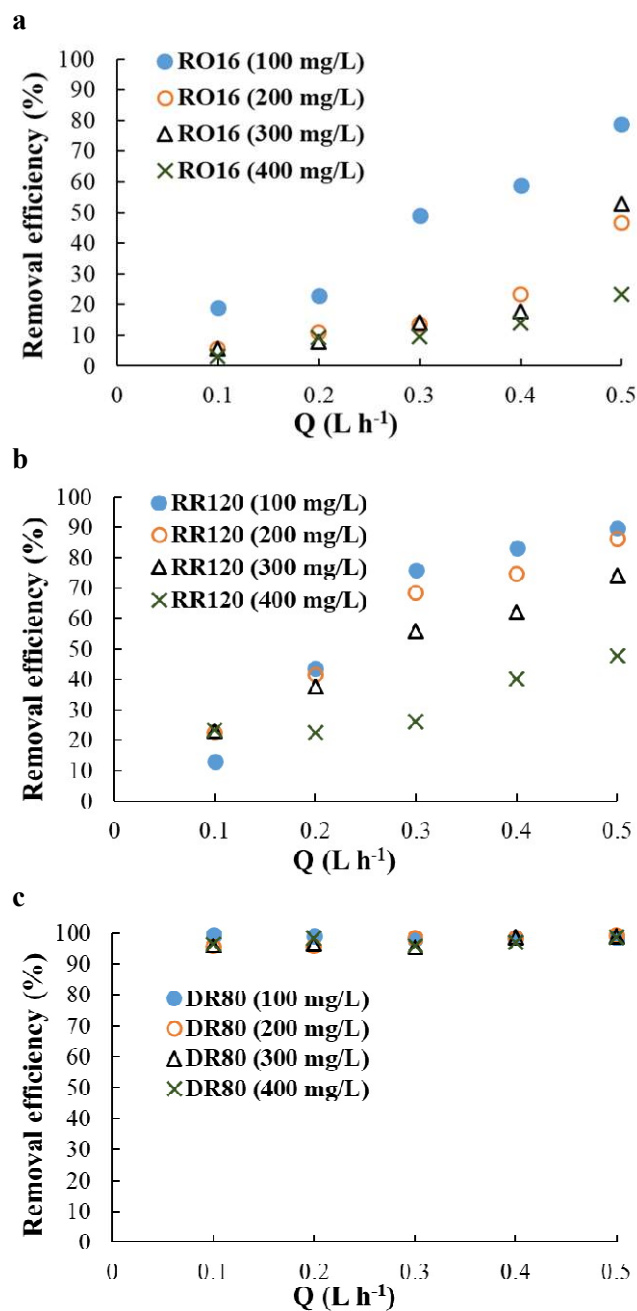


**Fig. 2** Effect of flow rate and inlet concentration on the removal efficiency of RO16 (a), RR120 (b) and DR80 (c) dyes

395

396 To deeper understand the influence of flow rate, a comparison between the applied  
 397 current density ( $j_{app}$ ) value (47 mA cm<sup>-2</sup>) with the initial limiting current density ( $j_{lim}^0$ ) values  
 398 has been performed by calculating the dimensionless current density ( $\alpha$ ), as defined by Eq.  
 399 (17) (Panizza et al., 2001):

400 
$$\alpha = \frac{j_{appl}}{j_{lim}^0} \quad (17)$$

401 In addition,  $j_{lim}^0$  can be expressed as function of Faraday constant (F), the mass  
 402 transport coefficient ( $k_m$ ) and the inlet COD ( $COD_{in}$ ) Eq. (18) (Panizza et al., 2001):

403 
$$j_{lim}^0 = 4Fk_mCOD_{in} \quad (18)$$

404 By combining Eqs. (17) - (18), the following relation of  $\alpha$  can be written Eq. (19):

405 
$$\alpha = \frac{j_{appl}}{4Fk_mCOD_{in}} \quad (19)$$

406 In order to determine  $\alpha$ , the value of  $k_m$  is required.  $k_m$  has been estimated considering  
 407 the dimensionless Sherwood (Sh) number relation that can be defined as function of  $k_m$ , the  
 408 equivalent diameter ( $d_h$ ) and the diffusivity (D) Eq. (20) (Cañizares et al., 2006):

409 
$$Sh = \frac{k_m d_h}{D} \quad (20)$$

410 Sh number can also be generally expressed as function of dimensionless Reynolds (Re)  
 411 number and Schmidt (Sc) number. Eq. (21) (Anglada et al., 2010)), while Sc is defined through  
 412 Eq. (22) (Cañizares et al., 2006) and Re in a stirred tank reactor can be determined considering  
 413 Eq. (23) (Fitschen et al., 2019):

414 
$$Sh = aRe^bSc^c \quad (21)$$

415 
$$Sc = \frac{\nu}{D} \quad (22)$$

416 
$$Re = \frac{a^2 N}{\nu} \quad (23)$$

417 where  $\nu$  is the kinematic viscosity, d is the diameter of the stirrer, N is the rotation speed of the  
 418 stirrer.

419 By combining Eqs. (20) - (23), the general expression of  $k_m$  is Eq. (24):

420 
$$k_m = \frac{a}{a_h} D^{(1-c)} \nu^{(c-b)} (d^2 N)^b \quad (24)$$

421 Finally, the general dimensionless  $\alpha$  relation in a stirred tank reactor is proposed as  
422 follow by combining Eq. (19) and Eq. (24):

$$423 \quad \alpha = \frac{j_{appl} \frac{d_h}{a}}{4FCOD_{in}} D^{(c-1)} v^{(b-c)} (d^2 N)^{-b} \quad (25)$$

424 In this work, the values of  $d_h$ ,  $d$ ,  $D$ ,  $N$ ,  $v$ ,  $a$ ,  $b$  and  $c$  constants were considered equalled  
425 to 10.5 cm, 2 cm,  $10^{-9} \text{ m}^2 \text{ s}^{-1}$  (Scialdone et al., 2012b), 100 rpm,  $8.917 \times 10^{-7} \text{ m}^2 \text{ s}^{-1}$  at 25°C  
426 (Engineering ToolBox, 2004), 0.228 (Selman and Tobias, 1978), 0.66 (Selman and Tobias,  
427 1978) and 0.33 (Selman and Tobias, 1978), respectively. A  $k_m$  value of  $1.7 \cdot 10^{-6} \text{ m s}^{-1}$  was  
428 therefore obtained in this study. This value is in the same range of values given in literature for  
429 a stirred tank reactor ( $\sim 5.9 \cdot 10^{-6} \text{ m s}^{-1}$ ) (dos Santos et al., 2014; Mousset et al., 2019b; Rocha et  
430 al., 2012). The  $COD_{in}$  values used for  $\alpha$  calculation are reported in Table SM-7. The results of  
431 dimensionless current density as function of the dyes and their inlet concentrations are  
432 displayed in Fig. 3b. In all the cases,  $\alpha$  was ranging from 18 to 102 and was always higher than  
433 1, which means that  $j_{appl}$  was always higher than  $j_{lim}^0$ . It can therefore be concluded that the  
434 kinetics were under mass transport control all along the treatment (Mousset et al., 2019a;  
435 Panizza et al., 2001). Knowing that the flow rate has an influence on  $k_m$ , it means that  
436 increasing  $Q$  make increase  $k_m$  and therefore enhance the kinetics, since it is under mass  
437 transport control. Thus, it explains the increase of removal efficiency with an increase of flow  
438 rate in Fig. 4.

439

440

441

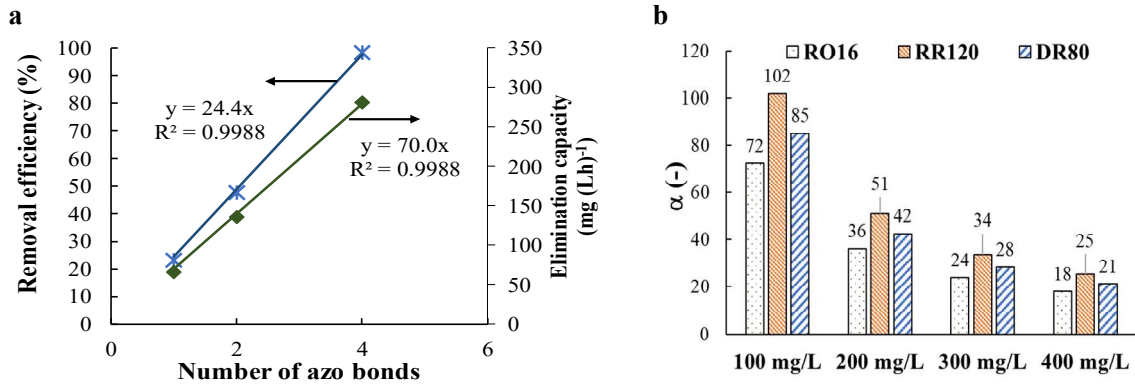
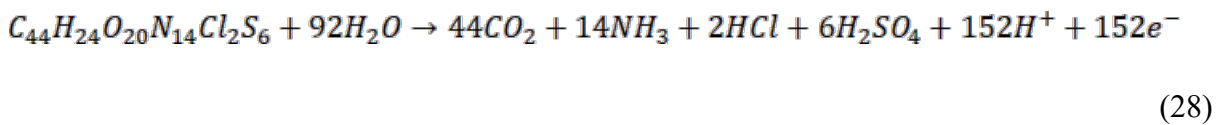
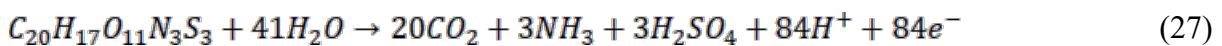


**Fig. 3** Influence of number of azo bonds on the dyes removal efficiency and elimination capacity at 400 mg L<sup>-1</sup> and 0.5 L h<sup>-1</sup> (a), dimensionless current density as function of inlet concentration of RO16, RR120 and DR80 dyes (b)

To further assess the efficiency of the process, the current efficiency (CE) has been calculated considering a continuous mode using Eq. (26) (Scialdone et al., 2012a):

$$CE (\%) = 100 \times \frac{nF C_{in} X Q}{j_{appl} A} \quad (26)$$

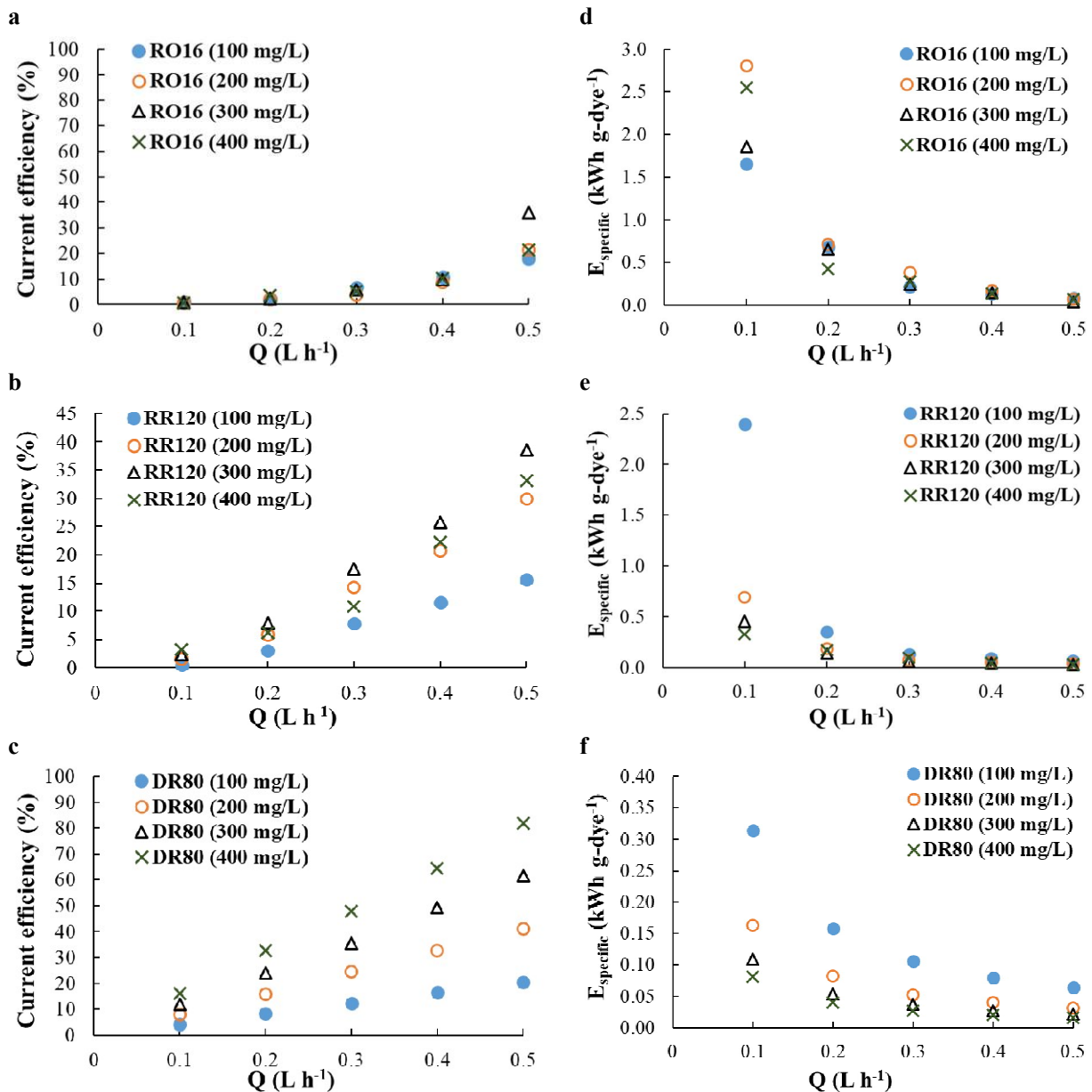
where A is the immersed surface area of the electrode (17 cm<sup>2</sup>), X is the conversion yield ((C<sub>in</sub> - C<sub>out</sub>)/C<sub>in</sub>) and n is the number of electron(s) required for the conversion of the dye into carbon dioxide by electrochemical combustion reaction that can be written as follow for RO16 (Eq. (27)), RR120 (Eq. (28)) and DR80 (Eq. (29)):



From Eqs. (27) - (29), it can be noted that the values of n for RO16, RR120, and DR80 were 84, 152 and 170, respectively. The specific electric energy consumption (E<sub>specific</sub>) was also estimated in continuous mode (Eq. (30)) (Mousset et al., 2018):

$$E_{specific} = \frac{E_{cell} I}{C_{in} X Q} \quad (30)$$

where,  $E_{\text{cell}}$  is the cell potential (V) and  $I$  is the current intensity (A).



462

463 **Fig. 4** Effect of flow rate and inlet concentration on the current efficiency (a, b, c) and the  
 464 specific energy requirement (d, e, f) to remove RO16 (a, d), RR120 (b, e) and DR80 (c, f) dyes

465

466 Both current efficiency and specific energy have been plotted in Fig. 4 as function of flow  
 467 rate and inlet concentration. The following rank of CE was obtained (from the highest to the  
 468 lowest): DR80 (4% - 82%) > RR120 (0.45% - 33%) > RO16 (0.56% - 21%), whatever the inlet  
 469 concentration and flow rate. This trend was in agreement with the removal efficiencies (Fig. 2).

470 The energy requirement followed the opposite relation order (from the highest to the lowest  
471  $E_{\text{specific}}$  value): RO16 (0.07 - 2.8 kWh g-dye<sup>-1</sup>) > RR120 (0.033 - 2.4 kWh g-dye<sup>-1</sup>) > DR80  
472 (0.016 - 0.31 kWh g-dye<sup>-1</sup>). At optimal condition for complete decolorization, the energy  
473 consumption was around 6 kWh m<sup>-3</sup> in this work against 11 kWh m<sup>-3</sup> with aluminium anode  
474 obtained in a previous study (Arslan-Alaton et al., 2008). This demonstrates the interest of  
475 using stainless steel anode compared to aluminium electrode.

476 In addition, CE and  $E_{\text{specific}}$  were generally raising and decreasing respectively with the  
477 inlet concentration, as a further confirmation of the kinetics dependency with the inlet  
478 concentration. Moreover, CE values were increasing with the flow rate, while  $E_{\text{specific}}$  values  
479 were decreasing, due to mass transport control.

480

#### 481 4. CONCLUSIONS

482 This study investigates the electrochemical decomposition of synthetic azo dyes (RO16,  
483 RR120 & DR80) using a continuous electrochemical reactor containing stainless steel  
484 electrodes. The interaction between the influencing parameters was determined using RSM.  
485 The results obtained from the transformed model showed that the optimum operating  
486 conditions for obtaining maximum percentage of dye decolorization were pH of 11.0  
487 electrolyte concentration of 0.5 M. The elimination capacity of electrochemical reactor was  
488 studied with respect to residence time for the continuous removal of azo dyes. The effect of  
489 other process parameters such as mass transport coefficient, dimensionless current density,  
490 current efficiency and specific energy were evaluated. The  $\alpha$  value given for the process shows  
491 that the global kinetics was under mass transport control. Current efficiency (%) increased for  
492 dyes with maximum number of azo bonds (irrespective of the initial dye concentration and  
493 flow rate) and the condition was vice versa with respect to specific energy calculation. From  
494 the kinetic analysis and transport modelling, in case of both the batch and continuous process,

495 it is evident that the percentage of removal efficiency is directly linked to the initial dye  
496 concentration, pH, flow rate and number of azo bonds. Thus the model developed in this  
497 research work shows a paramount feasibility of using stainless steel electrode for the  
498 continuous electrochemical decomposition of textile effluents containing azo dyes. Moreover,  
499 the experimental understanding on mass transport coefficient, dimensionless current density,  
500 current efficiency and specific energy give interesting information towards the efficiency and  
501 the reactor design optimization for upscaling the process. As a next step, since the kinetics  
502 seems to be under mass transport control, a further optimization of the reactor design would  
503 even increase the current performance, by intensifying the mass transport between the bulk and  
504 the surfaces of electrodes.

505

## 506 **5. ACKNOWLEDGEMENT**

507 The authors are grateful to Prof. Anant Achary, Department of Biotechnology, Kamaraj  
508 College of Engineering & Technology for providing us valuable suggestions in approaching  
509 this research work.

510

## 511 **6. REFERENCES**

- 512 Amani-ghadim, A.R., Aber, S., Olad, A., Ashassi-sorkhabi, H., 2013. Optimization of  
513 electrocoagulation process for removal of an azo dye using response surface methodology  
514 and investigation on the occurrence of destructive side reactions. *Chem. Eng. Process.*  
515 *Process Intensif.* 64, 68–78. <https://doi.org/10.1016/j.cep.2012.10.012>
- 516 Anglada, A., Urtiaga, A.M., Ortiz, I., 2010. Laboratory and pilot plant scale study on the  
517 electrochemical oxidation of landfill leachate. *J. Hazard. Mater.* 181, 729–35.  
518 <https://doi.org/10.1016/j.jhazmat.2010.05.073>
- 519 Aquino, J.M., Rocha-Filho, R.C., Rodrigo, M.A., Sáez, C., Cañizares, P., 2013.

520 Electrochemical degradation of the Reactive Red 141 dye using a boron-doped diamond  
521 anode. *Water. Air. Soil Pollut.* 224. <https://doi.org/10.1007/s11270-012-1397-9>

522 Arslan-Alaton, I., Kabdaşlı, I., Hanbaba, D., Kuybu, E., 2008. Electrocoagulation of a real  
523 reactive dyebath effluent using aluminum and stainless steel electrodes. *J. Hazard. Mater.*  
524 150, 166–173. <https://doi.org/10.1016/j.jhazmat.2007.09.032>

525 Bassyouni, D.G., Hamad, H.A., El-ashtoukhy, E.Z., Amin, N.K., El-latif, M.M.A., 2017.  
526 Comparative performance of anodic oxidation and electrocoagulation as clean processes  
527 for electrocatalytic degradation of diazo dye Acid Brown 14 in aqueous medium. *J.*  
528 *Hazard. Mater.* 335, 178–187. <https://doi.org/10.1016/j.jhazmat.2017.04.045>

529 Brahmi, L., Kaouah, F., Boumaza, S., Trari, M., 2019. Response surface methodology for the  
530 optimization of acid dye adsorption onto activated carbon prepared from wild date stones.  
531 *Appl. Water Sci.* 9. <https://doi.org/10.1007/s13201-019-1053-2>

532 Brillas, E., Martínez-Huitle, C.A., 2015. Decontamination of wastewaters containing synthetic  
533 organic dyes by electrochemical methods. An updated review. *Appl. Catal. B Environ.*  
534 166–167, 603–643. <https://doi.org/10.1016/j.apcatb.2014.11.016>

535 Cañizares, P., Marcos, I.F. De, Rodrigo, M.A., Lobato, J., 2006. Measurement of Mass-  
536 Transfer Coefficients by an Electrochemical Technique. *J. Chem. Educ.* 83, 1204–1207.  
537 <https://doi.org/10.1021/ed083p1204>

538 Correia, V.M., Stephenson, T., Judd, S.J., 1994. Characterisation of textile wastewaters - a  
539 review. *Environ. Technol. (United Kingdom)* 15, 917–929.  
540 <https://doi.org/10.1080/09593339409385500>

541 dos Santos, E.V., Sena, S.F.M., da Silva, D.R., Ferro, S., De Battisti, A., Martínez-Huitle,  
542 C.A., 2014. Scale-up of electrochemical oxidation system for treatment of produced water  
543 generated by Brazilian petrochemical industry. *Environ. Sci. Pollut. Res.* 21, 8466–8475.  
544 <https://doi.org/10.1007/s11356-014-2779-x>

545 Fitschen, J., Maly, M., Rosseburg, A., Wutz, J., Wucherpfennig, T., Schlüter, M., 2019.  
546 Influence of Spacing of Multiple Impellers on Power Input in an Industrial-Scale Aerated  
547 Stirred Tank Reactor. *Chemie-Ingenieur-Technik* 91, 1794–1801.  
548 <https://doi.org/10.1002/cite.201900121>

549 Gürses, A., Açıkyıldız, M., Güneş, K., Gürses, M.S., 2016. “Dyes and Pigments: Their  
550 Structure and Properties” in *SpringerBriefs in Green Chemistry for Sustainability* 13–29.  
551 <https://doi.org/10.1007/978-3-319-33892-7>

552 Hakizimana, J.N., Gourich, B., Chafi, M., Stiriba, Y., Vial, C., Drogui, P., Naja, J., 2017.  
553 Electrocoagulation process in water treatment: A review of electrocoagulation modeling  
554 approaches. *Desalination* 404, 1–21. <https://doi.org/10.1016/j.desal.2016.10.011>

555 Hasanbeigi, A., Price, L., 2015. A technical review of emerging technologies for energy and  
556 water efficiency and pollution reduction in the textile industry. *J. Clean. Prod.* 95, 30–44.  
557 <https://doi.org/10.1016/j.jclepro.2015.02.079>

558 Holkar, C.R., Jadhav, A.J., Pinjari, D. V, Mahamuni, N.M., Pandit, A.B., 2016. A critical  
559 review on textile wastewater treatments : Possible approaches. *J. Environ. Manage.* 182,  
560 351–366. <https://doi.org/10.1016/j.jenvman.2016.07.090>

561 Jegan Durai, N., Gopalakrishna, G.V.T., Padmanaban, V.C., Selvaraju, N., 2020. Oxidative  
562 removal of stabilized landfill leachate by Fenton’s process: Process modeling,  
563 optimization & analysis of degraded products. *RSC Adv.* 10, 3916–3925.  
564 <https://doi.org/10.1039/c9ra09415f>

565 Michaelis, L., 1935. Semiquinones, the intermediate steps of reversible organic oxidation-  
566 reduction. *Chem. Rev.* 16, 243–286. <https://doi.org/10.1021/cr60054a004>

567 Mohan, N., Balasubramanian, N., Basha, C.A., 2007. Electrochemical oxidation of textile  
568 wastewater and its reuse. *J. Hazard. Mater.* 147, 644–651.  
569 <https://doi.org/10.1016/j.jhazmat.2007.01.063>

570 Mousset, E., Pechaud, Y., Oturan, N., Oturan, M.A., 2019a. Charge transfer/mass transport  
571 competition in advanced hybrid electrocatalytic wastewater treatment: Development of a  
572 new current efficiency relation. *Appl. Catal. B Environ.* 240, 102–111.  
573 <https://doi.org/10.1016/j.apcatb.2018.08.055>

574 Mousset, E., Puce, M., Pons, M.-N., 2019b. Advanced electro-oxidation with boron-doped  
575 diamond for acetaminophen removal from real wastewater in a microfluidic reactor –  
576 Kinetics and mass transfer studies. *ChemElectroChem* 6, 2908–2916.  
577 <https://doi.org/10.1002/celec.201900182>

578 Mousset, E., Quackenbush, L., Schondek, C., Gerardin-Vergne, A., Pontvianne, S., Kmiotek,  
579 S., Pons, M.N., 2020. Effect of homogeneous Fenton combined with electron transfer on  
580 the fate of inorganic chlorinated species in synthetic and reclaimed municipal wastewater.  
581 *Electrochim. Acta* 334. <https://doi.org/10.1016/j.electacta.2019.135608>

582 Mousset, E., Wang, Z., Olvera-Vargas, H., Lefebvre, O., 2018. Advanced electrocatalytic pre-  
583 treatment to improve the biodegradability of real wastewater from the electronics industry  
584 — A detailed investigation study. *J. Hazard. Mater.* 360, 552–559.  
585 <https://doi.org/10.1016/j.jhazmat.2018.08.023>

586 Muniyasamy, A., Sivaporul, G., Gopinath, A., Lakshmanan, R., Altaee, A., Achary, A.,  
587 Velayudhaperumal Chellam, P., 2020. Process development for the degradation of textile  
588 azo dyes (mono-, di-, poly-) by advanced oxidation process - Ozonation: Experimental &  
589 partial derivative modelling approach. *J. Environ. Manage.* 265.  
590 <https://doi.org/10.1016/j.jenvman.2020.110397>

591 Nidheesh, P.V., Divyapriya, G., Oturan, N., Trelu, C., Oturan, M.A., 2019. Environmental  
592 Applications of Boron-Doped Diamond Electrodes: 1. Applications in Water and  
593 Wastewater Treatment. *ChemElectroChem* 6, 2124–2142.  
594 <https://doi.org/10.1002/celec.201801876>

595 Mousset, E., Oturan, N., Oturan, M.A., 2018. An unprecedented route of [rad]OH radical  
596 reactivity evidenced by an electrocatalytical process: Ipso-substitution with  
597 perhalogenocarbon compounds. *Appl. Catal. B Environ.* 226, 135–146.  
598 <https://doi.org/10.1016/j.apcatb.2017.12.028>

599 Padmanaban, V.C., Geed, S.R.R., Achary, A., Singh, R.S., 2016. Kinetic studies on  
600 degradation of Reactive Red 120 dye in immobilized packed bed reactor by *Bacillus*  
601 *cohnii* RAPT1. *Bioresour. Technol.* 213, 39–43.  
602 <https://doi.org/10.1016/j.biortech.2016.02.126>

603 Padmanaban, V.C., Selvaraju, N., Vasudevan, V.N., Achary, A., 2018. Augmented radiolytic  
604 (60Co) degradation of direct red 80 (Polyazo dye): optimization, reaction kinetics & G-  
605 value interpretation. *React. Kinet. Mech. Catal.* 125, 433–447.  
606 <https://doi.org/10.1007/s11144-018-1410-4>

607 Panizza, M., Cerisola, G., 2009. Direct and mediated anodic oxidation of organic pollutants.  
608 *Chem. Rev.* 109, 6541–6569. <https://doi.org/10.1021/cr9001319>

609 Panizza, M., Michaud, P.A., Cerisola, G., Comninellis, C., 2001. Anodic oxidation of 2-  
610 naphthol at boron-doped diamond electrodes. *J. Electroanal. Chem.* 507, 206–214.  
611 [https://doi.org/10.1016/S0022-0728\(01\)00398-9](https://doi.org/10.1016/S0022-0728(01)00398-9)

612 Rocha, J.H.B., Solano, A.M.S., Fernandes, N.S., da Silva, D.R., Peralta-Hernandez, J.M.,  
613 Martínez-Huitle, C.A., 2012. Electrochemical Degradation of Remazol Red BR and  
614 Novacron Blue C-D Dyes Using Diamond Electrode. *Electrocatalysis* 3, 1–12.  
615 <https://doi.org/10.1007/s12678-011-0070-1>

616 Schneider, K., Hafner, C., Jäger, I., 2004. Mutagenicity of textile dye products. *J. Appl.*  
617 *Toxicol.* 24, 83–91. <https://doi.org/10.1002/jat.953>

618 Scialdone, O., Galia, A., Guarisco, C., La Mantia, S., 2012a. Abatement of 1,1,2,2-  
619 tetrachloroethane in water by reduction at silver cathode and oxidation at boron doped

620 diamond anode in micro reactors. *Chem. Eng. J.* 189–190, 229–236.  
621 <https://doi.org/10.1016/j.cej.2012.02.062>

622 Scialdone, O., Galia, A., Randazzo, S., 2012b. Electrochemical treatment of aqueous solutions  
623 containing one or many organic pollutants at boron doped diamond anodes. Theoretical  
624 modeling and experimental data. *Chem. Eng. J.* 183, 124–134.  
625 <https://doi.org/10.1016/j.cej.2011.12.042>

626 Selman, J.R., Tobias, C.W., 1978. Mass-Transfer Measurements by the Limiting-Current  
627 Technique. *Adv. Chem. Eng.* 10, 211–318.

628 Shahnaz, T., S., M.M.F., V.C., P., Narayanasamy, S., 2020a. Surface modification of  
629 nanocellulose using polypyrrole for the adsorptive removal of Congo red dye and  
630 chromium in binary mixture. *Int. J. Biol. Macromol.* 151, 322–332.  
631 <https://doi.org/10.1016/j.ijbiomac.2020.02.181>

632 Shahnaz, T., Sharma, V., Subbiah, S., Narayanasamy, S., 2020b. Multivariate optimisation of  
633 Cr (VI), Co (III) and Cu (II) adsorption onto nanobentonite incorporated  
634 nanocellulose/chitosan aerogel using response surface methodology. *J. Water Process  
635 Eng.* 36. <https://doi.org/10.1016/j.jwpe.2020.101283>

636 Sharma, V., Shahnaz, T., Subbiah, S., Narayanasamy, S., 2020. New Insights into the  
637 Remediation of Water Pollutants using Nanobentonite Incorporated Nanocellulose  
638 Chitosan Based Aerogel. *J. Polym. Environ.* 28, 2008–2019.  
639 <https://doi.org/10.1007/s10924-020-01740-9>

640